Infrared Properties of High Redshift and X-ray Selected AGN Samples

Belinda J. Wilkes[1], Eric J. Hooper[1], Kim K. McLeod[2], Martin S. Elvis[1], David H. Hughes[3], Chris D. Impey[4], Joanna K. Kuraszkiewicz[1], Carol S. Lonsdale[5], Matt A. Malkan[6], and Jonathan C. McDowell[1]

[1] Harvard-Smithsonian CfA, Cambridge, MA 02138 USA
[2] Wellesley College, Wellesley, MA 02481 USA
[3] INAOE, Puebla, Pue. Mexico
[4] Steward Observatory, Tucson, AZ 85721 USA
[5] IPAC, Caltech, Pasadena, CA 91125 USA
[6] UCLA, Los Angeles, CA 90095-1562 USA

Abstract. The NASA/ISO Key Project on active galactic nuclei (AGN) seeks to better understand the broad-band spectral energy distributions (SEDs) of these sources from radio to X-rays, with particular emphasis on infrared properties. The ISO sample includes a wide variety of AGN types and spans a large redshift range. Two subsamples are considered herein: 8 high-redshift ($1 < z < 4.7$) quasars; and 22 hard X-ray selected sources.

The X-ray selected AGN show a wide range of IR continuum shapes, extending to cooler colors than the optical/radio sample of [7]. Where a far-IR turnover is clearly observed, the slopes are < 2.5 in all but one case so that non-thermal emission remains a possibility. The highest redshift quasars show extremely strong, hot IR continua requiring $\sim 100 M_\odot$ of 500–$1000\,K$ dust with ~ 100 times weaker optical emission. Possible explanations for these unusual properties include: reflection of the optical light from material above/below a torus; strong obscuration of the optical continuum; or an intrinsic deficit of optical emission. A cosmology of (H_0, Ω_m, Ω_k, Ω_Λ) = (50 km s^{-1} Mpc^{-1}, 1, 0, 0) is assumed.

1 Introduction

Active galactic nuclei are among the broadest emission sources in nature, producing significant flux over a span > 9 decades in frequency, from radio to X-rays and beyond [7]. The various emission mechanisms involved are presumably ultimately powered by a central supermassive black hole [28].

A substantial fraction of the bolometric luminosity of many AGN emerges in the infrared, from synchrotron radiation and dust. Which of these is the principal emission mechanism is related to quasar type and is an open question in many cases [37]. Non-thermal emission is paramount in core dominated radio-loud quasars and blazars [19], although hot dust contributes in some cases [4]. The non-thermal component is likely related to radio and higher frequency synchrotron radiation, providing information about the relativistic plasma and magnetic fields associated with quasars. Other AGN classes
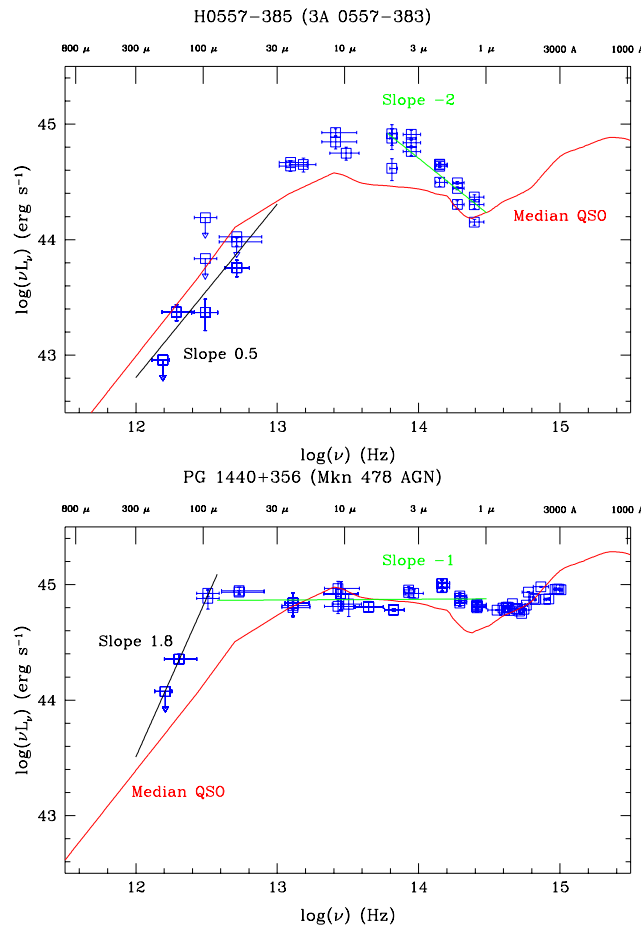
show evidence for a predominant dust contribution [6], particularly infrared-luminous radio-quiet quasars [15], or a mix of emission components [12]. Much of the dust emission is due to heating by higher energy photons from the active nucleus, and is therefore important for understanding the overall energy balance. The AGN thermal component may be an orientation-independent parameter, useful for examining unification hypotheses.

The nature of the foremost infrared emission source is ambiguous in many AGN with sparsely sampled spectral energy distributions (SEDs). Dust with smooth spatial and temperature distributions can mimic a power law spectrum [29,3], particularly in the absence of detailed measurements to reveal bumps from temperature and density inhomogeneities. Grain emissivity is characterized by a Planck function multiplied by a power law factor $\propto \nu^{1-2}$ [16], so spectral slopes in the Rayleigh-Jeans region of the coldest potential thermal component lie between $\alpha = 2$–4, depending on the grain properties and optical depth. Known synchrotron emitters have relatively flat sub-mm power-law spectra ($\alpha \leq 1.1; f_\nu \propto \nu^\alpha$) [10], and radio sources generally have spectra flatter than the canonical $\alpha = 2.5$ for a self-absorbed homogeneous synchrotron source [26]. Therefore, $\alpha = 2.5$ is a convenient partition to distinguish thermal emission from standard non-thermal models, and simple two-point spectral slopes and even lower limits to spectral indices may reveal the dominant mechanism. However, synchrotron models with a concave electron energy distribution [5,31], free-free absorption, or plasma suppression [32] can produce slopes steeper than $\alpha = 2.5$. While $\alpha = 4$ is observed in some milliarcsecond radio knots [24], thermal models offer the most consistent explanation for steep far-infrared (FIR) to mm slopes [15,1]. A thermal origin is considered to be the most likely explanation for sub-mm/FIR slopes $\alpha > 2.5$ in the present work.

Two large, complementary ISO AGN observing programs are opening up new wavelength windows in the FIR as well as improving the spatial resolution and sampling at shorter wavelengths: the ISO European Central Quasar Program [12,13]; and the NASA/ISO Key Project on AGN, discussed herein. The Key Project sample consists of 5–200 μm chopped and rastered ISOPHOT [22] observations of 73 AGN selected to incorporate a wide range of AGN types and redshifts. The data are reduced using a combination of the (ISO-) PHOT Interactive Analysis (PIA) [9] software plus custom scripts. Details of the reduction, difficulties encountered, and early results are discussed in [36,17,38,18]. These observations directly measure the FIR spectral slopes in low and moderate redshift AGN and provide better constraints on the emission mechanisms throughout the infrared region. Some of the fundamental questions being addressed with the new data include: the range of SEDs within each quasar type; differences between one type and another; the evolution of the SEDs; and correlations with fluxes at other wavebands, host galaxy properties, and orientation indicators. This paper focuses on two subsamples, hard X-ray selected AGN, and high-redshift quasars.

2   Hard X-ray Selected AGN

Infrared and X-ray data complement each other well and are important for understanding the overall AGN energy balance. Non-thermal infrared emission is possibly connected with the X-rays, either directly as a portion of a broad synchrotron component, or as part of a radio-infrared seed spectrum which Compton scatters to produce the X-rays. Infrared data from dust-dominated sources reveal the level of ultra-violet (UV) and soft X-ray radiation which has been reprocessed, and dust masses can be estimated assuming optically thin emission.

Fig. 1. *Spectral Energy Distributions (SEDs) of H0557-385 (top) and PG1440+356 (bottom) compared with the median SED for a low-redshift sample [7] illustrating the two extreme SED types present in this sample. The near-IR and far-IR cutoff slopes are indicated in both cases.*
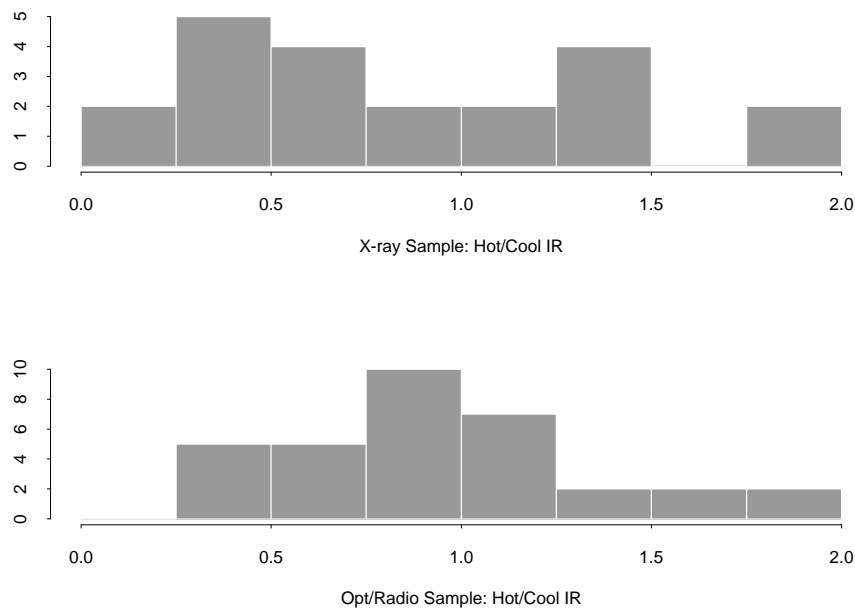
Table 1. X-ray Selected Sample: IR SED Parameters.

Name	z	$L_{10-100\mu}$ 10^{44} erg s^{-1}	$L_{1-10\mu}$ 10^{44} erg s^{-1}	α_{IR}	α_{cut}
MKN 1152	0.052	6.3	2.4	−0.9	−
MKN 590	0.025	3.3	4.2	−0.9	−
H0235−52	0.045	4.5	2.6	−1.6	0.2
H0557−385	0.034	11.9	3.8	−2.1	0.7
PG0804+761	0.100	37.1	53.0	−1.9	0.6
H1039−074	0.674	450.	190.	−	−
NGC 3783	0.009	1.3	1.6	−1.4	1.4
TON 1542	0.064	8.3	15.9	−1.7	−
IR1321+058	0.201	210.	6.4	−2.8	1.8
MCG-6-30-15	0.008	0.6	0.4	−1.6	1.3
IC4329A	0.014	5.4	20.3	− 0.8	
H1419+480	0.072	15.5	7.2	−1.3	0.3
PG1440+356	0.077	18.1	17.5	−1.1	1.8
H1537+339	0.330	72.3	42.7	−1.1	−
KAZ1803+676	0.136	20.9	31.0	−1.3	0.2
E1821+643	0.297	720.	550.	−1.1	2.5
H1834−653	0.013	1.2	0.3	−1.9	1.6
MKN 509	0.035	11.4	20.3	−1.0	2.2
NGC 7213	0.006	1.0	0.6	−	−
MR2251−178	0.068	18.4	23.6	−0.9	3.7
MCG-2-58-22	0.048	13.0	10.0	−0.9	2.5

Most X-ray selected AGN to date have been observed in soft energy bands
< 3.5 keV [33,35,14]. These surveys suffer obscuration biases similar to opti-
cal selection, due to the gas typically associated with dust. The absorption
cross-section drops steeply with increasing energy [39], so hard X-ray selec-
tion is much less affected by intervening material. Surveys in hard X-rays
arguably are the most efficient way to distinguish between accreting and
stellar sources [8] as well as the optimal method for defining a representative
sample of AGN [37]. A comparison between the UV/soft X-ray flux absorbed
and the IR emission provides an estimate of the relative importance of ac-
cretion and stellar power in AGN. We randomly selected 23 ISO targets (of
which 22 are reported in Table 1) from a 2–10 keV AGN sample derived from
the A2 experiment onboard the HEAO 1 satellite [11,20]; 12 of these are also
in the earlier Piccinotti sample [21,23,27] from the same experiment.

Figure 1 shows the IR−optical SEDs for two HEAO AGN illustrating
the wide range of behavior present. H0557−385 shows a strong hot compo-
nent with a steep near-IR slope ($\alpha_{ir} \sim -2$, $F_\nu \propto \nu^\alpha$) and a turnover which
is relatively flat. PG1440+356 shows a very flat optical−near-IR continuum
($\alpha_{ir} \sim -1$), a strong cool component compared with the low-redshift me-
dian [7] and a steeper turnover ($\alpha_{cut} \sim 1.8$) which, however, still remains
below the critical value of 2.5 indicating thermal emission. The range of IR
continua in the sample overlaps but extends to redder continua than an opti-

cal/radio selected sample [7]. This is apparent in the low mean for the near-IR slope, $\alpha_{IR} \sim -1.4 \pm 0.5$ compared with the Median SED value of -1.0 ± 0.3 and also the extension to cooler values of the ratio of decade luminosities: $\mathrm{L}(1-10\mu)/\mathrm{L}(10-100\mu) = 0.8 \pm 0.5$ compared with the radio/optical sample: 1.0 ± 0.8. The latter is also illustrated by comparison of the histograms in Figure 2. However a Kolmogorov-Smirnov test does not indicate a significant difference in the samples (P=18%). If real, this trend is an interesting extension to the lack of bias against red optical/UV continua in these sources. Confirmation awaits more systematic comparisons in an upcoming paper.
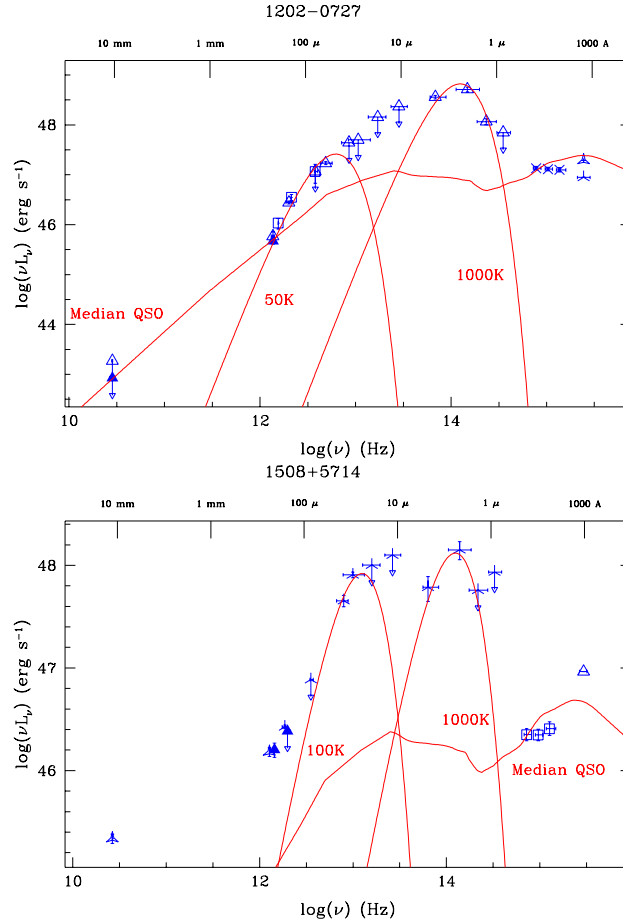

Fig. 2. *A comparison of the distribution of the ratio of hot to cool IR luminosities $(L(1-10\mu)/L(10-100\mu))$ for the HEAO sample with that of [7]. While a suggestive trend toward stronger cool luminosities is present in the HEAO sample, a KS test gives only an 18% probability that this is significant.*

3   High Redshift AGN

While skewed to low-redshift objects, due in part to lost sensitivity and changes in observing mode, the Key Project sample contains 8 quasars in the redshift range $1.0 \leq z \leq 4.7$. In order to cover the intrinsic FIR continuum in these sources, we also have an on-going sub-mm observing program at the JCMT.

The spectral energy distributions of these quasars vary widely. The highest redshift sources: $1202-0727$ ($z = 4.69$); $1508+5714$ ($z = 4.3$); and $1413+1143$ ($z = 2.551$), are factors of 10–100 brighter in the near-IR than the low-z

median SED [7] (Figure 3). At lower redshifts, PG1407+265 ($z = 0.944$) and PHL5200 ($z = 1.981$) are a much closer match to the median, while PG1718+481 ($z = 1.084$) is > 5 times fainter throughout the IR. A much larger sample will be required to determine the underlying distribution of SEDs at moderate and high-z which is hinted at by the variety seen here.

Fig. 3. *Spectral Energy Distributions (SEDs) of a) 1202−0727 and b) 1508+5714 compared with the median SED for a low-redshift sample [7] illustrating the extremely strong near-IR emission in both sources. Grey-body curves illustrating the minimum range of temperatures for purely thermal emission are also shown.*

The strong IR emission in the highest redshift quasars places them amongst the most powerful sources known. The range of temperatures is broad, 40–1000 K. Table 2 lists derived properties for two sources. The mass estimates assume optically thin gray dust with $\beta = 2$. The 40 K component in 1508+5714 is based on only the observed 850 μm flux; it is likely to be an

upper limit, because the FIR slope is flattening at those wavelengths, indicating possible contamination by a high frequency extension of the non-thermal radio emission. These and other high-redshift AGN [1,15,25] contain large amounts of dust, which implies a substantial star formation rate (SFR). Average SFRs listed in Table 2 were calculated from the inferred mass assuming a 1% dust production efficiency [2] and an onset of star formation at $z = 10$. Estimates of the FIR luminosity due solely to this SFR, computed with a conversion of $2.2 \times 10^9 \, L_\odot \, M_\odot^{-1}$ yr [30], are also listed. These are $\sim$ factor 10 below the observed luminosities, implying that the bulk of the FIR emission is driven by the AGN, or the sources are undergoing an intense starburst of $\geq 1000 \, M_\odot \, \mathrm{yr}^{-1}$.

Both sources have large excesses over the median SED in a spectral region that corresponds to warm and hot dust emission. This emission cannot yet be conclusively attributed to a thermal source, but that is a strong possibility, since cool dust is clearly present in $1202-0727$ and both objects show a sharp cutoff at wavelengths corresponding to the Wien region of dust near the sublimation temperature. The difficulty with a dust interpretation is the energy source to heat the material; the observed rest-frame optical and near-UV luminosity is clearly too low in both sources. Dust may obscure all but a small fraction $\sim 1\%$ of the intrinsic blue bump luminosity. It is unlikely that we are directly viewing the extincted source, as broad emission lines are clearly visible on continua which do not appear heavily reddened [34]. The observed flux may be diminished by reflection off of a scattering surface positioned above a dust torus. Alternatively, if we are seeing the intrinsic output of the central engine in the optical and near-UV, then these AGN must be abnormally luminous in the far-UV and X-rays. There is an indication of a blue upturn in 1508+5714, but the requisite luminosity remains unobserved.

Table 2. Properties of two High-Redshift Sources

Name	z	Dust Mass ($M_\odot$)			$\overline{\mathrm{SFR}}$	FIR($\overline{\mathrm{SFR}}$)
		$40\,K$	$100\,K$	$1000\,K$	($M_\odot\,\mathrm{yr}^{-1}$)	(10^{45} erg s^{-1})
$1202-0727$	4.690	1.5×10^9	$< 2.2 \times 10^7$	300	250	2.1
$1508+5714$	4.300	2.0×10^9	3.6×10^7	53	280	2.4

4 Summary

The principal points discussed in this paper are:

- The X-ray selected AGN show a broader, cooler range of IR continua than optical/radio selected AGN.
- The X-ray selected sample show no strong evidence ((MR2251$-$178 excepted) for a steep, $\alpha_{cut} > 2.5$, far-IR turnover, which would rule out non-thermal emission. Sub-mm observations are necessary to confirm.
- $z > 4$ quasars show $\sim$100 times stronger near-IR emission than low-z AGN. This may be due to strong obscuration, orientation or a real deficit of optical emission in these sources.

- The strong cool IR emission in the high-z sources implies dust masses $>$ $10^9\,M_\odot$, which would require an average SFR of a few hundred $M_\odot\,\mathrm{yr}^{-1}$. This underproduces the observed FIR flux, so there is either a major AGN component, or the SFR at the time of observation is significantly larger, $\geq 1000\,M_\odot\,\mathrm{yr}^{-1}$.

References

1. Andreani, P., Franceschini, A., & Granato, G. 1999, MNRAS, 306, 161
2. Blain, A. W., et al. 1999, MNRAS, 302, 632
3. Bollea, D., & Cavaliere, A. 1976, A&A, 49, 313
4. Courvoisier, T. J.-L. 1998, A&ARv, 9, 1
5. de Kool, M., & Begelman, M. C. 1989, Nat, 338, 484
6. Edelson, R. A., Malkan, M. A. 1987, ApJ, 323, 516
7. Elvis, M. S., et al. 1994, ApJS, 95, 1
8. Fiore, F., et al. 1999, MNRAS, 306, L55
9. Gabriel, C., et al. 1998, Proc. of ADASS VII, ASP Conf. Ser., 145, 165
10. Gear, W., et al. 1994, MNRAS, 267, 167
11. Grossan, B. A. 1992, Ph.D. Thesis, MIT
12. Haas, M., et al. 1998, ApJ, 503, 109L
13. Haas, M., et al. 1999, A&A, submitted
14. Hasinger, G., et al. 1998, A&A, 329, 482
15. Hughes, D. H., et al. 1993, MNRAS, 263, 607
16. Hildebrand, R. H. 1983, QJRAS, 24, 267
17. Hooper, E. J., et al. 1999, in The Universe as Seen by ISO, 893
18. Hooper, E. J., et al. 1999, ASP Conf. Ser. 177, 153
19. Impey, C. D., & Neugebauer, G. 1988, AJ, 95, 307
20. Jahoda, K., & Mushotzky, R. F. 1989, ApJ, 346, 638
21. Kotilainen, J. K., et al. 1992, MNRAS, 256, 149
22. Lemke, D., et al. 1996, A&A, 315, L64
23. Malizia, A., 1999, ApJ, 519, 637
24. Matveyenko, L. I., & Witzel, A. I. 1999, Ast Let, 25, 643
25. McMahon, R. G., et al. 1999, MNRAS, 309, L1
26. O'Dea, C. P. 1998, PASP, 110, 493
27. Piccinotti, G., et al. 1982, ApJ, 253, 485
28. Rees, M. J. 1984, ARAA, 22, 471
29. Rees, M. J., et al. 1969, Nat, 223, 788
30. Rowan-Robinson, M. 1997, MNRAS, 289, 490
31. Schlickeiser, R., Biermann, P. L., Crusius-Wätzel, A. 1991, A&A, 247, 283
32. Schlickeiser, R., & Crusius, A. 1989, IEEE Trans Plas Sci, 17, 245
33. Stocke, J. T., et al. 1991, ApJS, 76, 813
34. Storrie-Lombardi, L. J., et al. 1996, ApJ, 468, 121
35. Thomas, H. C., et al. 1998, A&A, 335, 467
36. Wilkes, B. J. 1997, in Quasar Hosts, 136
37. Wilkes, B. J. 1999, in Quasars & Cosmology, ASP Conf. Ser. 162, 15
38. Wilkes, B. J., et al. 1999, in The Universe as Seen by ISO, 845
39. Zombeck, M. V. 1990, Handbook of Space Astron. & Astrophys., 2nd Ed., 198